Available online at www.sciencedirect.com
ScienceDirect
Control Engineering Practice 15 (2007) 689–701
CONTROL ENGINEERING PRACTICE
www.elsevier.com/locate/conengprac

Study and implementation of an EKF GIB-based underwater positioning system

A. Alcocer*, P. Oliveira, A. Pascoal

Institute for Systems and Robotics and Department of Electrical Engineering, Instituto Superior Técnico, Av. Rovisco Pais, 1096 Lisboa Codex, Portugal

Available online 21 June 2006

Abstract

The paper addresses the problem of estimating the position of an underwater target in real time. In the scenario adopted, the target carries a pinger that emits acoustic signals periodically, as determined by a very high precision clock that is synchronized with GPS, prior to system deployment. The target is tracked from the surface by using a system of four buoys equipped with hydrophones and electronic circuitry that measures the times of arrival of the acoustic signals emitted by the pinger or, equivalently, the four target-to-buoy range measurements (a commercial version of this setup is the GIB system). Due to the finite speed of propagation of sound in water, these measurements are obtained with different latencies. The paper tackles the problem of underwater target tracking in the framework of extended Kalman filtering by relying on a purely kinematic model of the target. The paper further shows also how the differently delayed measurements can be merged using a *back and forward* fusion approach. A measurement validation procedure is introduced to deal with dropouts and outliers. Simulation as well as experimental results illustrate the performance of the filter proposed.

Keywords: Underwater vehicles; Navigation systems; Extended Kalman filters

1. Introduction

The last decade has witnessed the emergence of Ocean Robotics as a major field of research. Remotely operated vehicles (ROVs) and, more recently, autonomous underwater vehicles (AUVs) have shown to be extremely important instruments in the study and exploration of the oceans. Free from the constraints of an umbilical cable, AUVs are steadily becoming the tool *par excellence* to acquire marine data on an unprecedented scale and, in the future, to carry out interventions in undersea structures. Central to the operation of these vehicles is the availability of accurate navigation and positioning systems. The first provide measurements of the angular and linear position of a vehicle and are therefore crucial to platform stabilization and control. The latter include, but are not restricted to, systems that are designed with the sole purpose of tracking the evolution of an underwater platform from a surface ship. There is a clear connection between the two systems, for the latter can be used to complement information provided by a navigation system resident on-board the vehicle when a reliable acoustic communications link can be established between the surface and the underwater units. This paper focuses on the positioning problem defined above.

The fact that electromagnetic signals do not penetrate below the sea surface makes the GPS unsuitable for underwater positioning. Hence, alternative solutions must be sought. The good propagation characteristics of sound waves in water makes acoustic positioning a viable solution.

Classical approaches to underwater vehicle positioning include long baseline (LBL) and short baseline (SBL) systems, to name but a few. See Jouffroy and Opderbecke (2004), Kinsey and Whitcomb (2003), Larsen (2001), Leonard, Bennett, Smith, and Feder (1998), Milne (1983), Vaganay, Bellingham, and Leonard (1996), and the references therein for an introduction to this challenging area. More recently, a number of methods have been

*Corresponding author. Tel.: +351 218418051x81; fax: +351 218418291.
E-mail addresses: alexblau@isr.ist.utl.pt (A. Alcocer), pjcro@isr.ist.utl.pt (P. Oliveira), antonio@isr.ist.utl.pt (A. Pascoal).

0967-0661/$ - see front matter © 2006 Elsevier Ltd. All rights reserved.
doi:10.1016/j.conengprac.2006.04.001

proposed to "reproduce" the idea of GPS in the underwater environment. In Youngberg (1992) an underwater GPS concept was introduced. The system consists of surface buoys equipped with DGPS receptors that broadcast satellite information underwater, via acoustic telemetry. The underwater platform receives these messages from the buoys and computes its own position locally. Due to the technical difficulties inherent to acoustic communications, and as far as the authors are aware, this concept has not yet materialized in the form of a commercial product.

A different, yet related approach to acoustic underwater positioning has actually been implemented and is available commercially: the so-called GPS intelligent buoy (GIB) system (ACSA, 1999; Thomas, 1998). This system consists of four surface buoys equipped with DGPS receivers and submerged hydrophones. Each of the hydrophones receives the acoustic impulses emitted periodically by a synchronized pinger installed on-board the underwater platform and records their times of arrival (TOA). As explained later in Section 7, the depth of the target is also available from the GIB system by coding that info in the acoustic emission pattern. The buoys communicate via radio with a central station (typically on-board a support vessel) where the position of the underwater target is computed. Due to the fact that position estimates are only available at the central station, this system is naturally suited for tracking applications.

Motivated by the latter approach to acoustic positioning, this paper addresses the general problem of estimating the position of an underwater target given a set of range measurements from the target to known buoy locations. Classically, this problem has been solved by resorting to triangulation techniques (Henry, 1978), which require that at least three range measurements be available at the end of each acoustic emission–reception cycle. This is hardly feasible in practice, due to unavoidable communication and sensor failures. It is therefore of interest to develop an estimator structure capable of dealing with the case where the number of range measurements available is time-varying. The paper shows how this problem can be tackled in the framework of extended Kalman filtering (EKF), whereby four vehicle-to-buoy range measurements drive a filter that relies on a simple kinematic model of the underwater target.

It is important to recall that due to the finite speed of propagation of sound in water, the range measurements are obtained at the buoys with different latencies. To overcome this problem, the paper shows how the differently delayed measurements can be merged in an EKF setting by incorporating a *back and forward* fusion approach. Simulation as well as experimental results illustrate the performance of the filter proposed.

The paper is organized as follows. Section 2 describes the problem of underwater target positioning and introduces the relevant process and measurement models. Based on the models derived, Section 3 computes the matrices that are essential to the mechanization of a solution to the positioning problem in terms of an EKF. Section 4 shows how the EKF structure can be changed to accommodate latency in the measurements. Section 5 describes the acoustic validation and initialization procedures that were implemented for actual algorithm implementation. Simulation and experimental results that illustrate the performance of the filter proposed are discussed in Sections 6 and 7. Finally, Section 8 contains the main conclusions and describes challenging problems that warrant further research.

2. Problem statement. Filter design models

Consider an earth fixed reference frame $\{O\} \coloneqq \{X_0, Y_0, Z_0\}$ and four (possibly drifting) buoys at the sea surface with submerged hydrophones at positions $[x_{hi}(t)\ y_{hi}(t)\ z_{hi}(t)]^{\mathrm{T}}$; $i = 1, \ldots, 4$ as depicted in Fig. 1. For simplicity of presentation, we restrict ourselves to the case where the target moves in a plane at a fixed known depth $z_p(t)$. Its position in the earth fixed frame is therefore given by vector $[x(t)\ y(t)\ z_p(t)]^{\mathrm{T}}$. The problem considered in this paper can then be briefly stated as follows: obtain estimates $[\hat{x}(t)\ \hat{y}(t)]^{\mathrm{T}}$ of the target position based on information provided by the buoys, which compute the travel time of the acoustic signals emitted periodically by a pinger installed onboard the underwater platform. The solution derived can be easily extended to the case where the target undergoes motions in three-dimensional space.

2.1. Target (process) model

In what follows we avoid writing explicitly the dynamical equations of the underwater target being tracked and rely on its kinematic equations of motion only. Thus, a general solution for target positioning is obtained that fits different kinds of moving bodies such as AUVs, ROVs, divers, or even marine mammals.

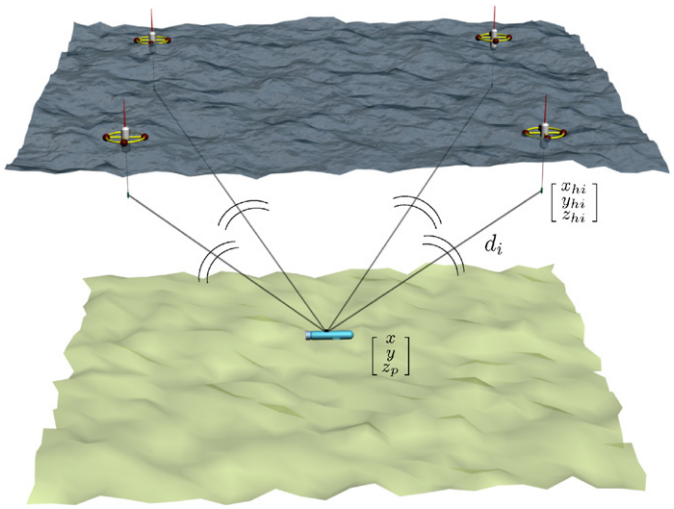

Fig. 1. The GIB system.

The following notation will be used in the sequel: V is the total velocity of the vehicle in $\{O\}$, ψ denotes the angle between vector V and X_0, and r is the derivative of ψ (see Fig. 2). Notice that the case where the target moves in three-dimensional space can be cast in the framework adopted in this paper if the depth coordinate can be measured independently. Under these circumstances, V should be re-interpreted as the projection of the total velocity vector on its two first components. Given a continuous-time variable $u(t)$, $u(t_k)$ denotes its values taken at discrete instants of time $t_k = kh; k \in Z_+$, where $h>0$ denotes the sampling interval. For reasons that will become evident later, it is not convenient to introduce the standard abbreviation $u(k)$ for $u(t_k)$. Simple arguments lead to the discrete-time kinematic model for the target

$$\begin{cases} x(t_{k+1}) = x(t_k) + hV(t_k)\cos\psi(t_k), \\ y(t_{k+1}) = y(t_k) + hV(t_k)\sin\psi(t_k), \\ V(t_{k+1}) = V(t_k) + w_v(t_k), \\ \psi(t_{k+1}) = \psi(t_k) + hr(t_k) + w_\psi(t_k), \\ r(t_{k+1}) = r(t_k) + w_r(t_k), \end{cases} \tag{1}$$

where the inclusion of the angular rate equation for $r(t_k)$ captures the fact that the target undergoes motions in ψ that are not measured directly and are thus assumed to be unknown. The process noises $w_v(t_k)$, $w_\psi(t_k)$, and $w_r(t_k)$ are assumed to be stationary, independent, zero-mean, and Gaussian, with constant standard deviations σ_v, σ_ψ, and σ_r, respectively. The above model can be written as a linear parametrically varying system of the form

$$\begin{aligned} \mathbf{x}(t_{k+1}) &= f(\mathbf{x}(t_k), \mathbf{w}(t_k)) \\ &= \mathbf{A}(\mathbf{x}(t_k))\mathbf{x}(t_k) + \mathbf{L}\mathbf{w}(t_k), \end{aligned} \tag{2}$$

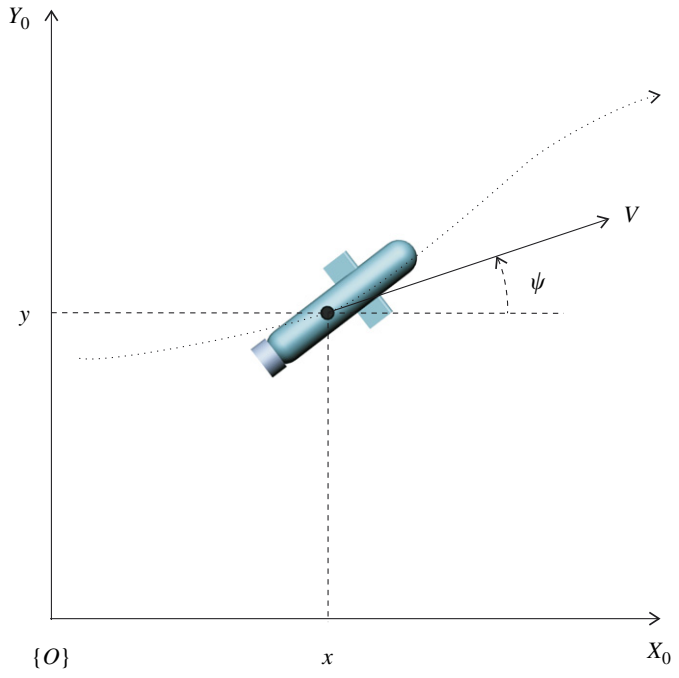

Fig. 2. Target model.

where

$$\mathbf{x}(t_k) = [x(t_k)\ y(t_k)\ V(t_k)\ \psi(t_k)\ r(t_k)]^{\mathrm{T}}, \tag{3}$$

$$\mathbf{w}(t_k) = [w_v(t_k)\ w_\psi(t_k)\ w_r(t_k)]^{\mathrm{T}}, \tag{4}$$

$$\mathbf{A}(\mathbf{x}(t_k)) = \begin{bmatrix} 1 & 0 & h\cos\psi(t_k) & 0 & 0 \\ 0 & 1 & h\sin\psi(t_k) & 0 & 0 \\ 0 & 0 & 1 & 0 & 0 \\ 0 & 0 & 0 & 1 & h \\ 0 & 0 & 0 & 0 & 1 \end{bmatrix},$$

$$\mathbf{L} = \begin{bmatrix} 0 & 0 & 0 \\ 0 & 0 & 0 \\ 1 & 0 & 0 \\ 0 & 1 & 0 \\ 0 & 0 & 1 \end{bmatrix}, \tag{5}$$

and

$$\mathrm{E}[\mathbf{w}(t_k)\mathbf{w}^{\mathrm{T}}(t_k)] \triangleq \mathbf{Q} = \begin{bmatrix} \sigma_v^2 & 0 & 0 \\ 0 & \sigma_\psi^2 & 0 \\ 0 & 0 & \sigma_r^2 \end{bmatrix}. \tag{6}$$

2.2. Measurement model

In the setup adopted for vehicle positioning the underwater pinger carries a high precision clock that is synchronized with those of the buoys (and thus with GPS) prior to target deployment. The pinger emits an acoustic signal every T seconds, at precisely known instants of time. To avoid a proliferation of symbols, only one period of interrogation will be examined in detail, the extension to the full time interval being trivial. See Fig. 3. Let s (at the beginning of an interrogation cycle) denote an arbitrary time at which the pinger emits a signal. In response to this excitation, the buoys $i; i = 1, \ldots, 4$ compute their distances d_i to the underwater unit at times $r_i \geqslant s$; $r_i = s + N_i h$, where

$$d_i(s) = \sqrt{(x_{hi} - x(s))^2 + (y_{hi} - y(s))^2 + (z_{hi} - z_p)^2} \tag{7}$$

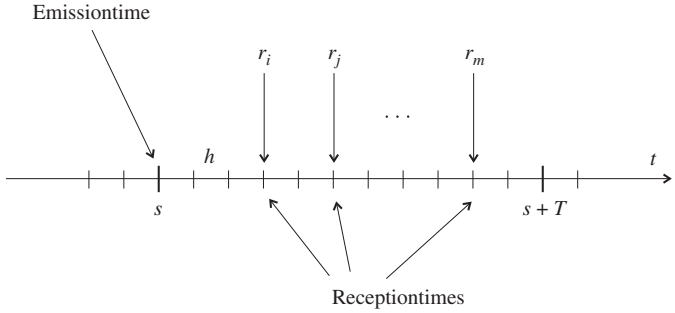

Fig. 3. Delayed observations. An acoustic pulse is generated at emission time s and observations computed at later times $r_1, \ldots, r_m$.

and N_i is the time it takes for the acoustic signal to reach buoy i, modulo the sampling interval h. In the above equation, x and y denote the horizontal coordinates of the pinger at time s. In general, the argument of x_{hi}, y_{hi}, x_{hi} is s. If the buoys are moored and approximately stationary, then the dependence on s vanishes. In what follows, it is assumed that $\max_i N_i h \leqslant T$, that is, all the receptions at the buoys arrive during an interrogation cycle.

Notice that the N_i's are not necessarily ordered by increasing order of magnitude, since they depend on the distance of each of the buoys to the target. Notice also that even though $z_i = z_i(s)$ refers to time s, its value can only be accessed at time $r_i > s$. It is therefore convenient to define $\bar{z}_i(r_i) = z_i(r_i - N_i h) = z_i(s)$, that is, $\bar{z}_i(r_i)$ is the measurement of $z_i(s)$ obtained at a later time r_i. With the above notation, the model adopted for the noisy measurements $z_i(s)$ of $d_i(s)$ is

$$z_i(s) = d_i(s) + (1 + \eta d_i(s))v_i(s), \tag{8}$$

where $v_i(s)$ is a stationary, zero-mean, Gaussian white noise process with constant standard deviation σ_i. It is assumed that $v_i(s)$ and $v_j(s)$ are independent for $i \neq j$. The constant parameter η captures the fact that the measurement error increases as the range d_i grows.

The full set of available measurements available over an acoustic emission cycle can vary from 0 to 4, depending on the conditions of the acoustic channel. Mathematically, the set of $0 \leqslant m \leqslant 4$ measurements can be written as

$$\mathbf{z}^m(s) \triangleq \mathscr{C}[z_1(s) \ \cdots \ z_4(s)]^{\mathrm{T}}, \tag{9}$$

where $\mathscr{C} : \mathscr{R}^4 \to \mathscr{R}^m$ denotes the operator that extracts the m entries in $[z_1(s) \ \cdots \ z_4(s)]^{\mathrm{T}}$ that are actually available and orders them according to the time-sequence at which they are computed at the buoys. Missing entries are simply ignored. Again, it is important to emphasize that even though the information contained in $\mathbf{z}^m(s)$ refers to time s, it is available in a scattered manner over the interrogation cycle. For clarity of exposition it is convenient to introduce the vector $\mathbf{z}^p(s)$; $p \leqslant m$ that is obtained from $\mathbf{z}^m(s)$ by keeping its first p components. It is also convenient to define

$$\mathbf{v}^m(s) \triangleq \mathscr{C}[v_1(s) \ \cdots \ v_4(s)]^{\mathrm{T}}, \tag{10}$$

$$\mathbf{R}^m \triangleq \mathrm{E}[\mathbf{v}^m(s)\mathbf{v}^{mT}(s)] = \mathrm{diag}\{\mathscr{C}[\sigma_1 \ \cdots \ \sigma_4]^{\mathrm{T}}\}. \tag{11}$$

3. Extended Kalman filter design

In preparation for the development that follows, consider for the time being the "ideal" situation where all or part of the m measurements obtained over an interrogation cycle are available at the corresponding interrogation time s, as condensed in vector $\mathbf{z}^p(s)$; $p \leqslant m$. The procedure adopted to lift this assumption will become clear later. In this case, given the nonlinear process and the observation models given by (1) and (8), respectively it is simple to derive an EKF structure to provide estimates of positions $x(k)$ and $y(k)$ based on measurements $\mathbf{z}^p(s)$, where s denotes an arbitrary interrogation time. The details are omitted; see, for example, Anderson and Moore (1979) and the references therein. Following standard practice, the derivation of an EKF for the design model (2) builds on the computation of the following Jacobian matrices about estimated values $\hat{\mathbf{x}}(t_k)$ of the state vector $\mathbf{x}(t_k)$; $t_k = s, s+h, \ldots, s+T$:

$$\hat{\mathbf{A}}(\hat{\mathbf{x}}(t_k)) = \left.\frac{\partial f(\mathbf{x},\mathbf{w})}{\partial \mathbf{x}}\right|_{\hat{\mathbf{x}}(t_k)}, \quad \hat{\mathbf{L}}(\hat{\mathbf{x}}(t_k)) = \left.\frac{\partial f(\mathbf{x},\mathbf{w})}{\partial \mathbf{w}}\right|_{\hat{\mathbf{x}}(t_k)}, \tag{12}$$

$$\hat{\mathbf{C}}(\hat{\mathbf{x}}(s)) = \left.\frac{\partial \mathbf{z}^p}{\partial \mathbf{x}}\right|_{\hat{\mathbf{x}}(s)}, \quad \hat{\mathbf{D}}(\hat{\mathbf{x}}(s)) = \left.\frac{\partial \mathbf{z}^p}{\partial \mathbf{v}}\right|_{\hat{\mathbf{x}}(s)}. \tag{13}$$

Notice that the matrices $\hat{\mathbf{C}}(\hat{\mathbf{x}}(s))$ (abbv. $\hat{\mathbf{C}}(s)$) and $\hat{\mathbf{D}}(\hat{\mathbf{x}}(s))$ (abbv. $\hat{\mathbf{D}}(s)$) are only computed at $t = s$, that is, at the beginning of the interrogation cycle. It is straightforward to compute

$$\hat{\mathbf{A}}(\hat{\mathbf{x}}(t_k)) = \begin{bmatrix} 1 & 0 & h\cos(\hat{\psi}(t_k)) & -h\hat{V}(t_k)\sin(\hat{\psi}(t_k)) & 0 \\ 0 & 1 & h\sin(\hat{\psi}(t_k)) & h\hat{V}(k)\cos(\hat{\psi}(t_k)) & 0 \\ 0 & 0 & 1 & 0 & 0 \\ 0 & 0 & 0 & 1 & h \\ 0 & 0 & 0 & 0 & 1 \end{bmatrix} \tag{14}$$

and $\hat{\mathbf{L}} = \mathbf{L}$. Furthermore, by defining

$$\hat{C}_i(\hat{\mathbf{x}}(s)) = \left[-\frac{1}{\hat{z}_i(s)}(x_{hi} - \hat{x}(s)) \ \ -\frac{1}{\hat{z}_i(s)}(y_{hi} - \hat{y}(s)) \ 0 \ 0 \ 0 \right] \tag{15}$$

with

$$\hat{z}_i(s) = \sqrt{(x_{hi} - \hat{x}(s))^2 + (y_{hi} - \hat{y}(s))^2 + (z_{hi} - z_p)^2} \tag{16}$$

and

$$\hat{D}_i(\hat{\mathbf{x}}(s)) = 1 + \eta \hat{z}_i(s), \tag{17}$$

it follows that

$$\hat{\mathbf{C}}(\hat{\mathbf{x}}(s)) = stack^p\{\hat{C}_j(\hat{\mathbf{x}}(s))\} \tag{18}$$

where $stack^p$ denotes the operation of stacking p row matrices $\hat{C}_j(\hat{\mathbf{x}}(s))$; $j = 1, \ldots, p$ by re-ordering the sequence of sub-indices j to match the sequence in $\mathbf{z}^p(s)$. For example, if the distances measured by buoys 1, 2, and 3 are obtained according to the sequence 1, 3, 2, then

$$\hat{\mathbf{C}}(\hat{\mathbf{x}}(s)) = \begin{bmatrix} \hat{C}_1(\hat{\mathbf{x}}(s)) \\ \hat{C}_3(\hat{\mathbf{x}}(s)) \\ \hat{C}_2(\hat{\mathbf{x}}(s)) \end{bmatrix}. \tag{19}$$

Similarly,

$$\hat{\mathbf{D}}(\hat{\mathbf{x}}(s)) = diag^p\{\hat{D}_i(\hat{\mathbf{x}}(s)\}, \tag{20}$$

where the elements of the $p \times p$ diagonal matrix $\hat{\mathbf{D}}(\hat{\mathbf{x}}(s))$ are ordered in an analogous manner. Note that the dimensions of $\hat{\mathbf{C}}(s)$ and $\hat{\mathbf{D}}(s)$ vary according to the number of measurements that are available at time s.

The matrices $A(\hat{\mathbf{x}}(t_k))$ and $\hat{A}(\hat{\mathbf{x}}(t_k))$ defined before have the following important property that will be used later.

Property 1. *Given any nonzero positive integer N, define*

$$\begin{cases} \alpha_1 = \alpha_1(N,t_k) & \triangleq \sum_{l=0}^{N} \cos(\hat{\psi}(t_k) + l\hat{r}(t_k)), \\ \alpha_2 = \alpha_2(N,t_k) & \triangleq \sum_{l=0}^{N} \sin(\hat{\psi}(t_k) + l\hat{r}(t_k)), \\ \beta_1 = \beta_1(N,t_k) & \triangleq \sum_{l=0}^{N} l\cos(\hat{\psi}(k) + l\hat{r}(k)), \\ \beta_2 = \beta_2(N,t_k) & \triangleq \sum_{l=0}^{N} l\sin(\hat{\psi}(k) + l\hat{r}(t_k)). \end{cases} \tag{21}$$

Then it can be shown that

$$\hat{\mathbf{\Phi}}(t_k + Nh, t_k) \triangleq \prod_{l=0}^{N} \hat{\mathbf{A}}(\hat{\mathbf{x}}(t_k + lh)) = \begin{bmatrix} 1 & 0 & h\alpha_1 & -h\hat{V}(t_k)\alpha_2 & -h\hat{V}(t_k)\beta_1 \\ 0 & 1 & h\alpha_2 & h\hat{V}(t_k)\alpha_1 & h\hat{V}(t_k)\beta_2 \\ 0 & 0 & 1 & 0 & 0 \\ 0 & 0 & 0 & 1 & hN \\ 0 & 0 & 0 & 0 & 1 \end{bmatrix} \tag{22}$$

and

$$\mathbf{\Phi}(t_k + Nh, t_k) \triangleq \prod_{l=0}^{N} \mathbf{A}(\hat{\mathbf{x}}(t_k + lh)) = \begin{bmatrix} 1 & 0 & h\alpha_1 & 0 & 0 \\ 0 & 1 & h\alpha_2 & 0 & 0 \\ 0 & 0 & 1 & 0 & 0 \\ 0 & 0 & 0 & 1 & hN \\ 0 & 0 & 0 & 0 & 1 \end{bmatrix}. \tag{23}$$

For $N = 0$,

$$\hat{\mathbf{\Phi}}(t_k, t_k) = \mathbf{\Phi}(t_k, t_k) \triangleq \mathbf{I}. \tag{24}$$

4. Fusing delayed measurements with the EKF

In the previous section it was assumed that all buoy measurements are available at time s, when the interrogation cycle starts. This unrealistic assumption must be lifted in view of the variable time-delay affecting each buoy measurement. The question then arises as to how delayed measurements can be naturally incorporated into an EKF structure. The reader will find in Larsen, Poulsen, Andersen, and Ravn (1998) a survey of different methods proposed in the literature to fuse delayed measurements in a linear Kalman filter structure. In Larsen et al. (1998), a new method is also presented that relies on "extrapolating" the measurement of a variable obtained with latency to present time, using past and present estimates of the Kalman filter. The problem tackled in this paper differs from that studied in Larsen et al. (1998) in two main aspects: the underlying estimation problem is nonlinear, and the components of the output vector that refers to s are accessible with different latencies. As shown below, this problem can be addressed using a *back and forward* fusion approach which recomputes the filter estimates every time a new measurement is available, as depicted in Fig. 4. The computational complexity involved in the algorithm derived is drastically reduced by resorting to Property 1.

In this work the estimator runs at a sampling period h typically much smaller than T, the interrogation period of the underwater pinger. As before, let s be an arbitrary instant of time at which the underwater pinger emits an acoustic signal and let $i \leqslant m$ be the buoy that first receives this signal at time $r_i = s + N_i h$. Further, let $\bar{z}_i(r_i)$ be the corresponding distance. Up until time r_i no new measurements are available, and a pure state and covariance prediction update are performed using the EKF setup described before, leading to the *predictor*

$$\hat{\mathbf{x}}(t_{k+1}) = \mathbf{A}(\hat{\mathbf{x}}(t_k))\hat{\mathbf{x}}(t_k), \tag{25}$$

$$\mathbf{P}(t_{k+1}) = \hat{\mathbf{A}}(\hat{\mathbf{x}}(t_k))\mathbf{P}(t_k)\hat{\mathbf{A}}^{\mathrm{T}}(\hat{\mathbf{x}}(t_k)) + \hat{\mathbf{L}}\mathbf{Q}\hat{\mathbf{L}}^{\mathrm{T}} \tag{26}$$

with $t_k = s, s+h, \ldots, r_i$, where $\hat{\mathbf{x}}(t_k)$ and $\mathbf{P}(t_k)$ are the state prediction and the error prediction covariance, respectively. Upon reception of the first measurement $\bar{z}_i(r_i)$ available during the interrogation cycle, and assuming that the state $\hat{\mathbf{x}}(s)$ and covariance $\mathbf{P}(s)$ at time s have been stored, it is possible to go back to that initial time and perform a *filter state and covariance update* as if the measurement $\bar{z}_i(r_i)$ were in fact available at time s. Using the notation introduced before with $p = 1$ and $\mathbf{z}^p(s) = \bar{z}_i(r_i)$, it is straightforward to compute the update equations

$$\hat{\mathbf{x}}^+(s) = \hat{\mathbf{x}}(s) + \mathbf{K}(s)[\mathbf{z}^p(s) - \hat{\mathbf{z}}^p(s)], \tag{27}$$

$$\mathbf{P}^+(s) = \mathbf{P}(s) - \mathbf{P}(s)\hat{\mathbf{C}}^{\mathrm{T}}(s) \times [\hat{\mathbf{C}}(s)\mathbf{P}(s)\hat{\mathbf{C}}^{\mathrm{T}}(s) + \hat{\mathbf{D}}(s)\mathbf{R}^p\hat{\mathbf{D}}^{\mathrm{T}}(s)]^{-1}\hat{\mathbf{C}}(s)\mathbf{P}(s), \tag{28}$$

$$\mathbf{K}(s) = \mathbf{P}^+(s)\hat{\mathbf{C}}^{\mathrm{T}}(s)[\hat{\mathbf{D}}(s)\mathbf{R}^p\hat{\mathbf{D}}^{\mathrm{T}}(s)]^{-1}, \tag{29}$$

where $\hat{\mathbf{z}}^p(s)$ denotes the estimate of $\bar{\mathbf{z}}^p(s)$ obtained in the previous interrogation cycle. A new prediction cycle can now be done moving forward in time until a new

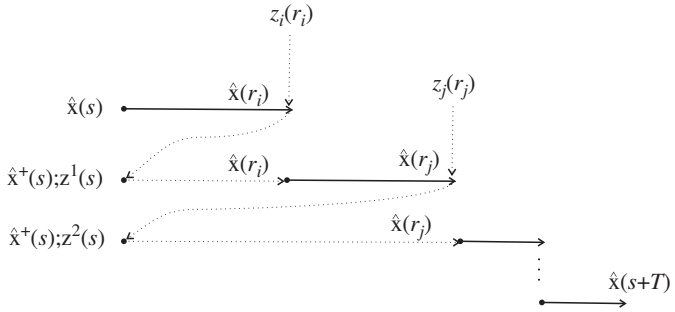

Fig. 4. *Back and forward* fusion approach. The solid line denotes the availability of real time outup filter data.

measurement z_j is available. This is done using (25)–(26) and starting with the updated states and covariance found in (27)–(28). Due to Property 1, this prediction can be expressed in a computationally simple form. Let $r_j = s + N_j h$ be the time step at which measurement $\bar{z}_j(r_j)$ is received. Then, the prediction cycle from s to r_j can be computed in closed form as

$$\hat{\mathbf{x}}(r_j) = \mathbf{\Phi}(r_j, s)\hat{\mathbf{x}}^+(s), \tag{30}$$

$$\mathbf{P}(r_j) = \hat{\mathbf{\Phi}}(r_j, s)\mathbf{P}^+(s)\hat{\mathbf{\Phi}}^{\mathrm{T}}(r_j, s) + \sum_{l=0}^{N_j-1} \hat{\mathbf{\Phi}}(s + lh, s)\mathbf{L}\mathbf{Q}\mathbf{L}^{\mathrm{T}}\hat{\mathbf{\Phi}}^{\mathrm{T}}(s + lh, s). \tag{31}$$

Again, upon computation of measurement $\bar{z}_j(r_j)$, it is possible to go back to time s and perform a filter state and covariance update as if measurements $\bar{z}_i(r_i)$ and $\bar{z}_j(r_j)$ were available at s. This is done using Eqs. (27)–(28), with the one-dimensional vector $\mathbf{z}^1(s)$ replaced by $\mathbf{z}^2(s) = [\bar{z}_i(r_i), \bar{z}_j(r_j)]^{\mathrm{T}}$ and matrices $\hat{\mathbf{C}}(s)$, $\hat{\mathbf{D}}(s)$, and $\mathbf{R}^2$ re-computed accordingly. This *back and forward* structure proceeds until the m measurements available over an interrogation cycle (starting at s and ending at $s + T$) are dealt with. The procedure is then repeated for each interrogation cycle. The overall structure of the algorithm proposed is depicted in Fig. 4.

5. Measurement validation and EKF initialization

In preparation for actual tests of the GIB-based system at sea, this section discusses practical issues that warrant careful consideration. As is well known, the implementation of any acoustic positioning system requires that mechanisms be developed to deal with dropouts and outliers that arise due to acoustic path screening, partial system failure, and multipath effects. See, for example, Vaganay, Leonard, and Bellingham (1996) and the references therein for an introduction to this circle of ideas and for an interesting application to AUV positioning using a LBL system. In the case of the GIB system, the problem is further complicated because of the mechanism that is used to transmit the depth of the target. In fact, the pinger onboard the vehicle emits two successive acoustic pulses during each emission cycle, the time delay between the two pulses being proportional to the pinger depth. Ideally, the data received at each buoy during each emission cycle consists of two successive pulses only. In practice, a number of pulses may be detected (even though the GIB system only provides 3) depending on the "quality" of the acoustic channel. For example, the data received may correspond to a number of situations that include the following or a combination thereof: (i) only the first pulse is received—a valid range measurement is acquired but the depth info is not updated, (ii) only the second pulse is received—data contains erroneous information, and (iii) a single pulse is received as a consequence of multipath effects—data may be discarded or taken into consideration if a model for multipath propagation is available.

In the present case, following the general strategy outlined in Vaganay, Leonard et al. (1996), a two-stage procedure was adopted that includes a time-domain as well as a spatial-domain validation. Time-domain validation is done naturally in an EKF setting by examining the residuals associated with the measurements (i.e., the difference between predicted and measured values as they arrive), and discarding the measurements with residuals that exceed a certain threshold. In this work the threshold is fixed and chosen before system deployment, according to the quality of the acoustic channel. We remark that there is a great potential for the inclusion of a time-varying threshold to improve the performance and robustness of the time-domain validation strategy. See, for example, Bar-Shalom and Fortmann (1988), Mili, Cheniae, Vichare, and Rousseeuw (1996), and the references therein for a lucid presentation of the circle of ideas that can be exploited in future work.

During system initialization, or when the tracker is not driven by valid measurements over an extended period of time, a spatial-domain validation is performed to overcome the fact that the estimate of the target position may become highly inaccurate. This is done via an initialization algorithm that performs multiple least squares (LS) triangulations based on all possible scenarios compatible with the set of measurements received and selects the solution that produces the smallest residuals.

The diagram in Fig. 5 depicts the complete procedure for measurement validation. In an initialization scenario, or

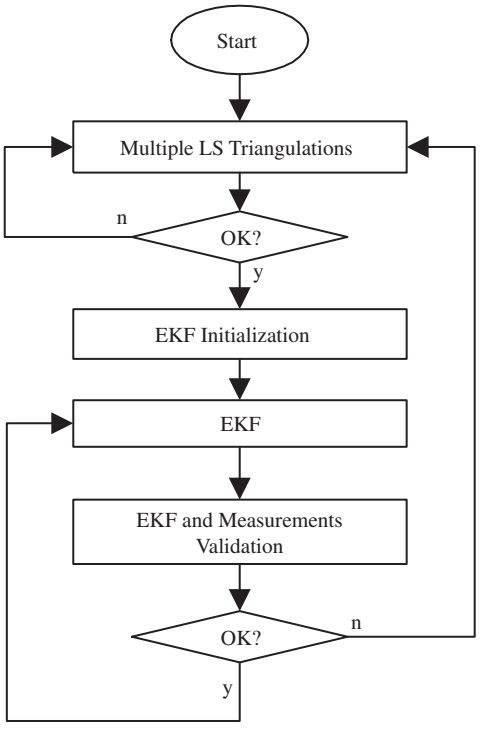

Fig. 5. Measurement validation and initialization procedures.

whenever a filter reset occurs, the multiple triangulation algorithm is performed until a valid solution is obtained, that is, until the residuals of the resulting set of measurements are less than a certain threshold. Once a valid position fix is obtained, the EKF is initialized and a procedure that relies on the EKF estimates and a priori information about the vehicle's maximum speed and noise characteristics selects the valid measurements. The EKF will be reset if the residuals become bigger than a threshold or if the duration of a pure prediction phase (that is, the time window during which no validated measurements are available) lasts too long.

For the sake of clarity, Fig. 6 is included here to show the type of raw and validated measurements that are obtained during real operations at sea. See Section 7 for a description of the tests where four buoys and an underwater pinger were deployed. At this point, however, it is sufficient to bring attention to some interesting details on the TOA of the acoustic pulses at one of the buoys, during an interrogation cycle. The vertical scale is in milliseconds to stress the fact that the buoy computes its distance to the pinger indirectly, by measuring the time-delay between the reception and the emission of the first acoustic pulse. As explained before, the GIB system provides a set of three detects over each interrogation cycle. In the figure, these detects tend to concentrate on two parallel curves that correspond to the times of reception of the two successive pulses that are emitted by the underwater unit (recall that the depth information is coded in the time-delay between the two emissions). However, there are other detects that cannot be explained by this mechanism.

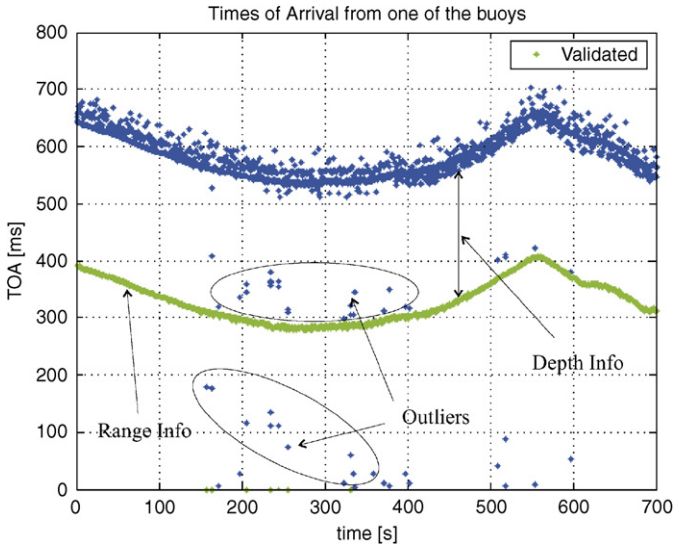

Fig. 6. Times of arrival (TOA) of acoustic pulses at one buoy. Zero values indicate that data were not available. Depth information is coded in the time between two consecutive pulses in each emission cycle.

6. Simulations

This section describes the results of simulations aimed at assessing the efficacy of the algorithms derived. In the simulations, four buoys were placed at the corners of a square with a 1 km side. The depth of the hydrophones z_{hi} was set to 5 m for all the buoys. The target was assumed to move at 1 m/s speed along segments of straight lines and

Table 1
Simulation filter parameters

$\mathbf{x}(0)$	$[500\ 400\ 1\ \pi/4\ 0]^{\mathrm{T}}$
$\hat{\mathbf{x}}(0)$	$[520\ 380\ 0.5\ \pi/2\ 0]^{\mathrm{T}}$
$\mathbf{P}(0)$	$\mathrm{diag}\{[(20)^2\ (20)^2\ (0.5)^2\ (0.05)^2\ (0.005)^2]\}$
σ_v	0.001
σ_ψ	0.005
σ_r	0.02
σ_i	$0.1, \quad i = 1,\ldots,4$
η	0.001

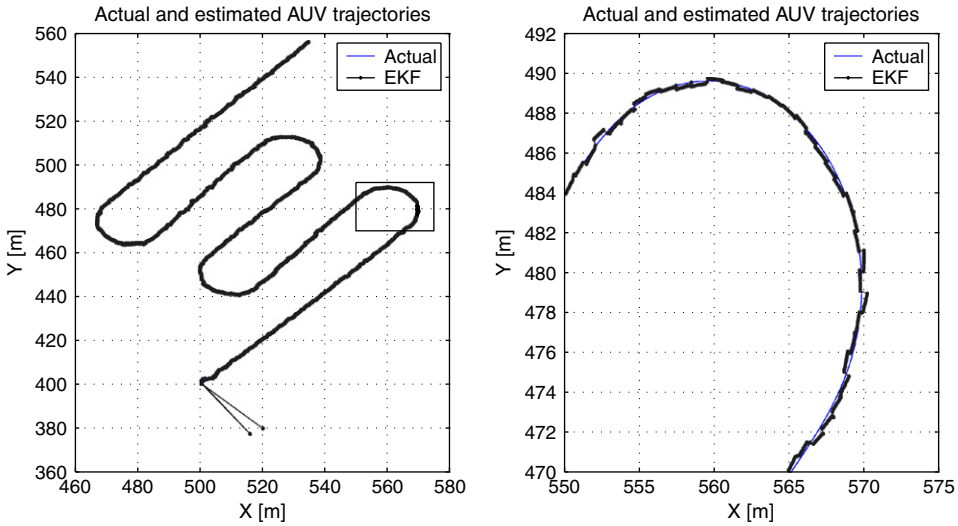

Fig. 7. Left: simulated and estimated AUV trajectories. Right: idem, zoom-in on boxed area.

circumferences with a 15 m diameter; see Fig. 7. The motion of the target was restricted to the horizontal plane, at a constant depth $z_p = 50$ m. The range measurements were generated every $T = 1$ s and corrupted by Gaussian measurement noise as in (8) with 0.1 m^2 standard deviation. The EKF was run at a sampling period of $h = 0.1$ s.

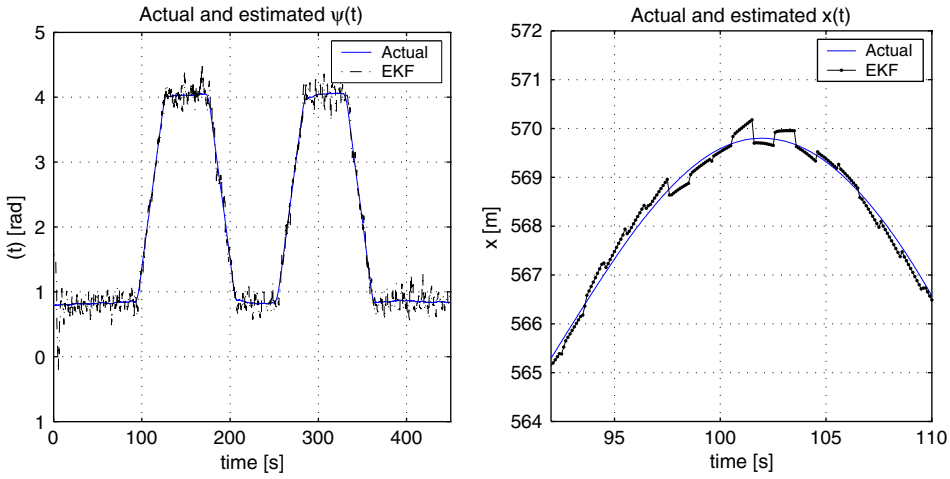

Fig. 8. Left: simulated and estimated $\psi(t)$. Right: detail of simulated and estimated $x(t)$.

Fig. 9. The IRIS platform with its arm retracted. The yellow unit can be easily replaced with a support for the GIB pinger (Courtesy of L. Sebastião).

Fig. 10. GIB buoys (left) and GIB pinger (right) (Courtesy of J. Alves).

The actual and estimated initial states, as well as the process and measurement noise intensities, are shown in Table 1.

Fig. 7 shows a simulation of actual and estimated two-dimensional target trajectories and the details of a turning maneuver. Fig. 8 shows actual and estimated $\psi(k)$ as well as the details of actual and estimated $x(k)$. Notice the "jump" in the estimates whenever a new measurement is available. Notice, however how the heading estimates change slowly in the course of a turning maneuver because the positioning system incorporates an internal model for the evolution of yaw rate r. At this point, it is also important to recall that all estimates of the target motion are computed using acoustic range measurements only. In spite of this, the performance of the filter is quite good.

7. Experimental setup and results

Evaluating the performance of an underwater positioning system is not an easy task due to the absence of simple procedures capable of yielding very accurate data against which to gage the precision of the position estimates. In some cases, reference positions are produced by off-line smoothing of actual observations, which is clearly far from ideal. Another possible strategy is to use a high frequency LBL to perform such an evaluation (Whitcomb, Yoerger, & Singh, 1999). In this work, a different setup was adopted by mounting the GIB underwater pinger on the IRIS surveying tool seen in Fig. 9, developed in the scope of the MEDIRES project for automated inspection of both the emerged and submerged parts of rubble-mound breakwaters (Silva et al., 2003). The IRIS tool consists of a Inertial Measurement Unit (Seatex MRU-6), two GPS receivers (Ashtech DG14) with the respective antennas carefully installed and calibrated at the bow and stern of the survey vessel, and an underwater body carrying a mechanical scanning pencilbeam sonar (Tritech SeaKing). A GPS receiver (Ashtech DG14) is also installed inshore and calibrated to provide corrections in the post-processing phase. Based on the GPS data acquired, both onboard and inshore, and using commercially available post-processing tools, the location of the underwater unit can be obtained with an accuracy in the horizontal better than 10 cm. For our purposes, the scanning sonar was simply replaced by the GIB pinger. Experimental raw data were acquired using a commercially available GIB system in Sines, Portugal, 24th June 2004, during a campaign of the MEDIRES project at the Sines West breakwater. Four buoys with submerged hydrophones at nominal depth of 10 m were moored in a square configuration with approximately 500 m on the side. Fig. 10 shows two GIB buoys together with their hydrophones and the GIB pinger attached to a modification of the IRIS structure.

A Matlab-based software application was implemented with functions to read and process the raw data from the GIB system log files. These files contain the TOA of the sound waves at each of the hydrophones and the buoy positions given by their respective GPS receivers. Because the rate at which data are acquired and processed is low, the positioning algorithm runs on a simple PC using

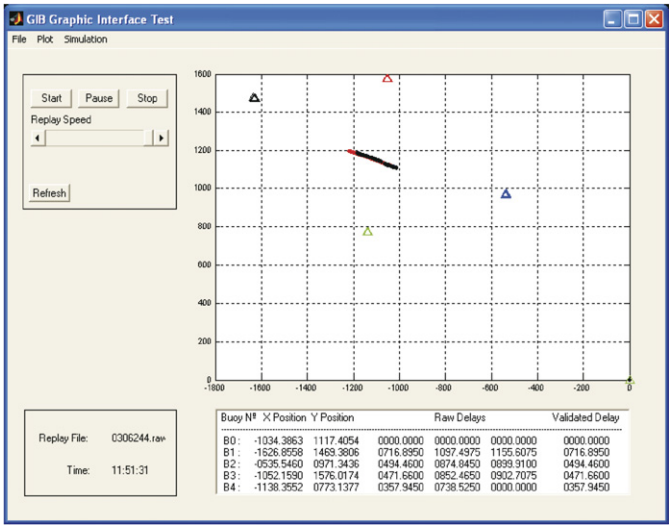

Fig. 11. Screenshot of positioning system/user interface.

Table 2
Experimental filter parameters

$\mathbf{P}(0)$	$\text{diag}\{[(25)^2\ (25)^2\ (1)^2\ (1)^2\ (0.005)^2]\}$
σ_v	$1.58e-2$
σ_ψ	$1.58e-2$
σ_r	$2.5e-10$
σ_i	4 if DGPS, 10 if GPS, $\quad i=1,\ldots,4$
η	$1e-3$

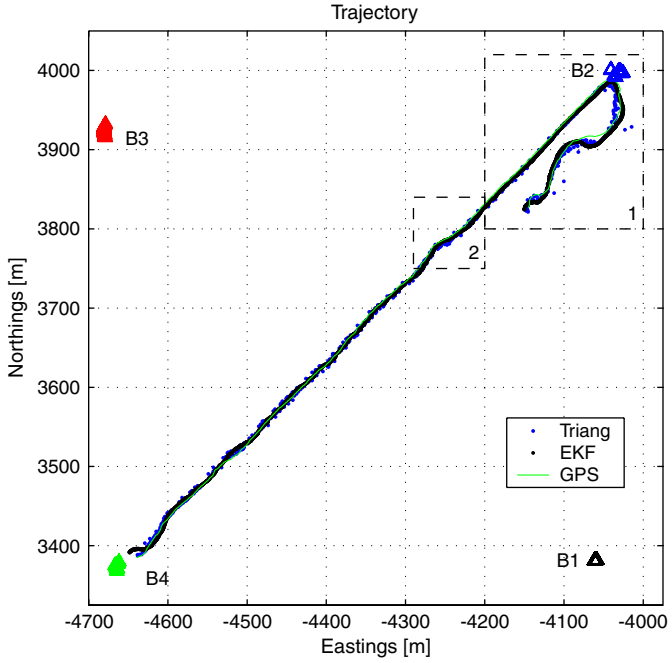

Fig. 12. Experimental trajectory.

Matlab. This has proven also sufficient for real-time processing. Fig. 11 is a screenshot of the graphical interface developed to report the status of the proposed algorithm and track the pinger underwater. Table 2 shows the filter parameters that were used in the mechanization of the positioning algorithm described in the paper. The interrogation cycle T was set to 1 s. The sampling time h for the filter was 0.1 s.

The actual experimental trajectory of the pinger and its estimates can be seen in Fig. 12. Details are shown in Fig. 13. In the figures, EKF stands for data obtained with the positioning algorithm proposed, Triang stands for Triangulation fixes, and GPS is the post-processed position reference obtained with the IRIS surveying tool. Note that Triangulation fixes are only computed when three or more validated observations are available.

Fig. 14 shows the positions of the buoys given by GPS. Notice that there is no data from buoy 2 until $t \approx 550$ s into this segment of the mission. Notice also the large jumps in position on the order of 10 m which are reflected into errors of the underwater positioning system.

Fig. 15 shows the TOA for all buoys. Notice that buoy 2 started transmitting data only at the end of the experiment. Events of this kind can and will occur during real

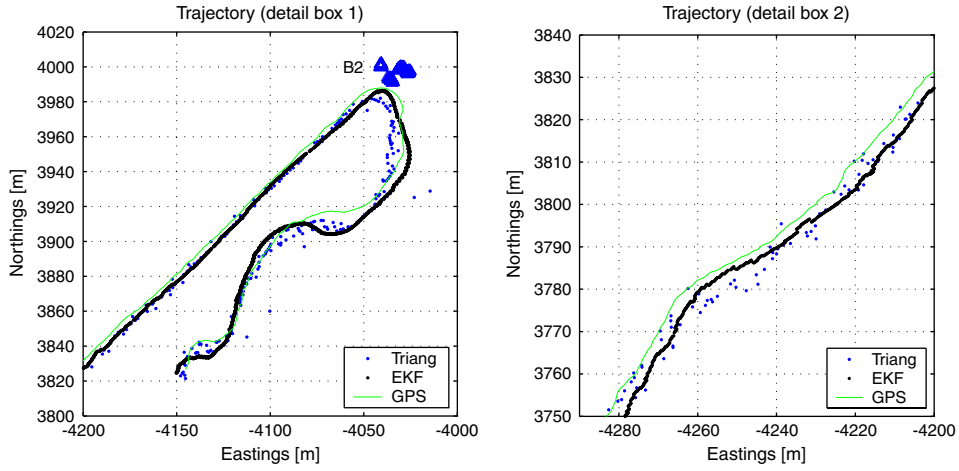

Fig. 13. Experimental trajectory (detail).

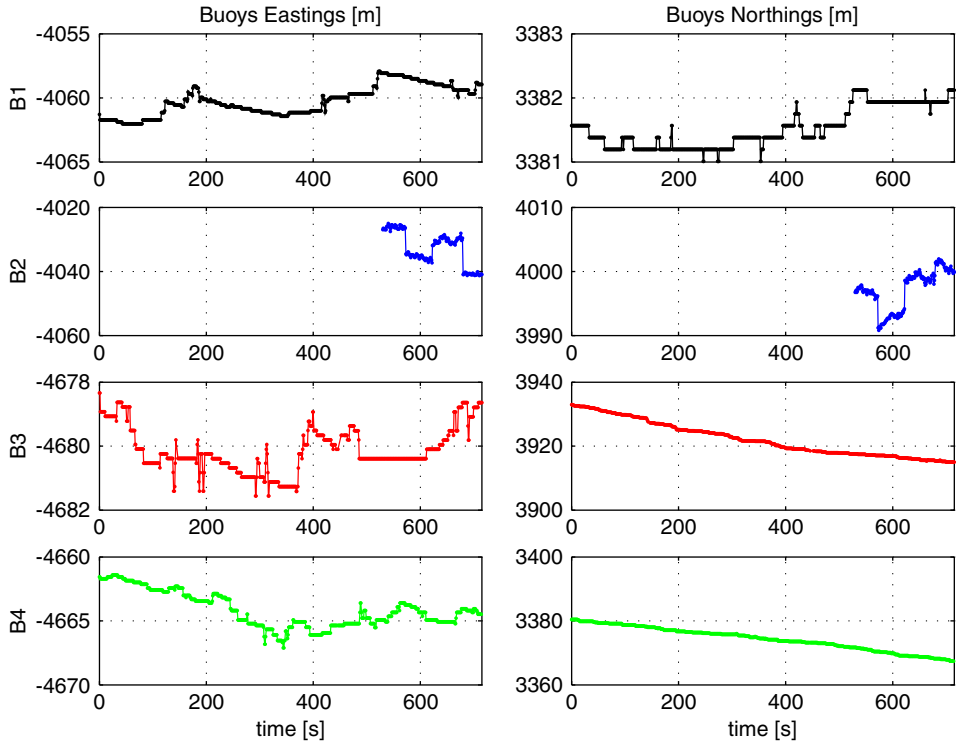

Fig. 14. Buoy positions given by GPS.

operations at sea. Later, it will be seen how even in the presence of such a dramatic failure the positioning system can still provide good estimates of the underwater target position. Fig. 16 is the enlargement of regions 1 and 2 in Fig. 15, that is, of the TOA for buoys 1 and 4. The upper and lower figures correspond to the same time interval and are shown on equal scales. Notice that the TOA for buoy 1 are much more noisier than those for buoy 2. Careful analysis suggests that multiple acoustic paths are being detected.

The number of raw and validated observations during the trajectory is shown in Fig. 17. Again, notice that buoy 2 starts to broadcast data only during the turn in the trajectory, which implies that the straight line between buoys 4 and 2 was done with a maximum of three observations available. There is an almost constant error of about 2 m between the positions obtained either by EKF or Triangulation and the ones given by IRIS which can be observed in Fig. 13. One possible source for this error is the fact that the hydrophones might not have been in the

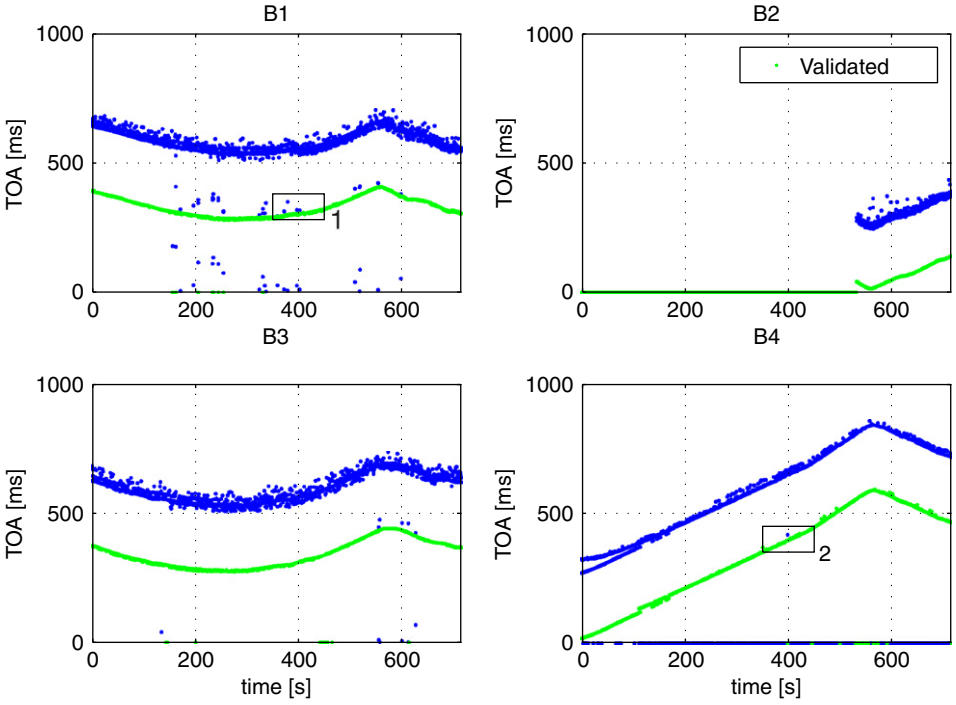

Fig. 15. Times of arrival at each of the buoys. Validated data in green.

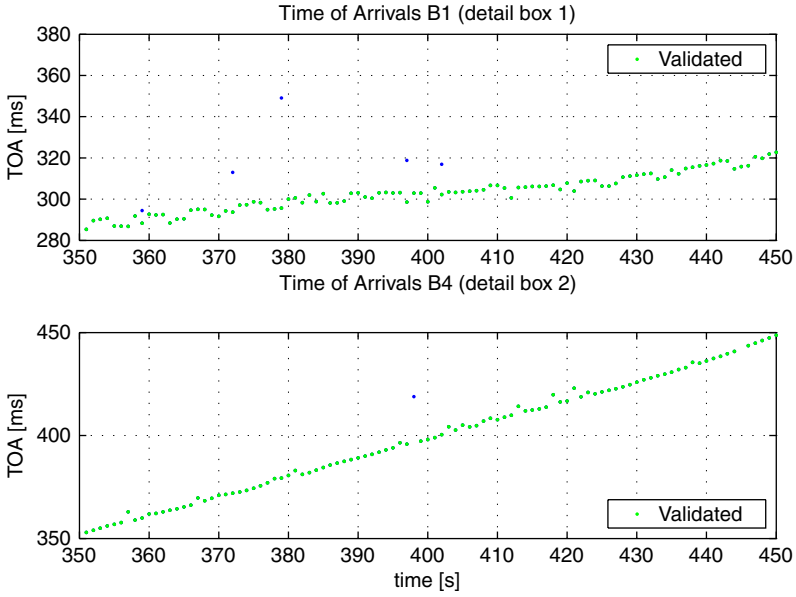

Fig. 16. Detail of times of arrival at buoys 1 and 4.

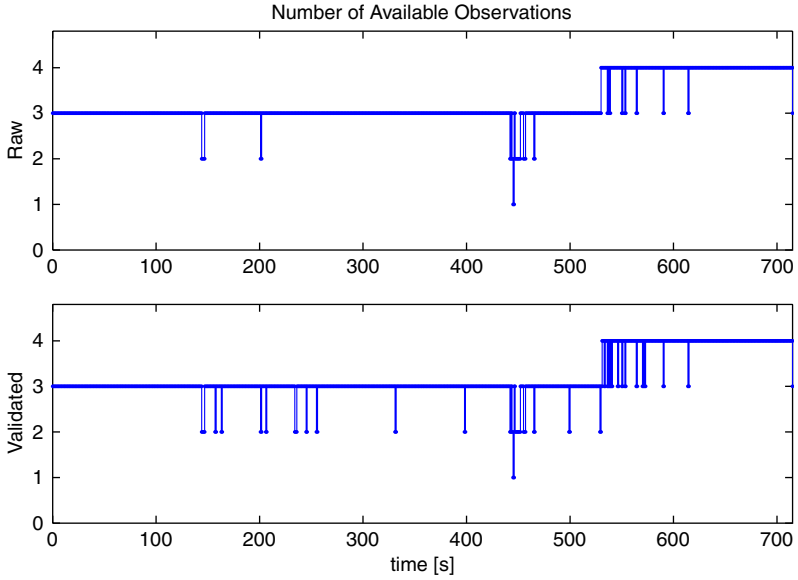

Fig. 17. Number of available (raw and validated) observations. Only three observations were available until time $t \approx 550$ s, when data from buoy 2 started being available.

vertical directed along the vertical axis of the buoy, due to currents. One important issue that has not been mentioned so far is the estimation of sound speed. It is obviously of extreme importance to have an accurate estimate of its value since it is used in the process of transforming differences in the TOA into distances. An estimate of the sound speed was determined using a simple LS algorithm that minimized the residuals of a set of triangulation fixes at the beginning of the experiments.

Fig. 18 shows the RMS position estimation error of EKF and Triangulation when compared to the post-processed GPS. Clearly, the algorithm proposed yields far better performance than triangulation. The figure does not give total justice to this fact, because it does not reflect the fact that the triangulation fixes are often not available due to bad quality of the data. In fact, only good triangulation data were considered. Furthermore, because the ratio $T/h = 10$ of the EKF filter rate versus the rate of the triangulation updates is large, the samples used to assess the performance of the EKF filter far exceed those used in the triangulation. Again, this fact is not mirrored in Fig. 18 (Table 3).

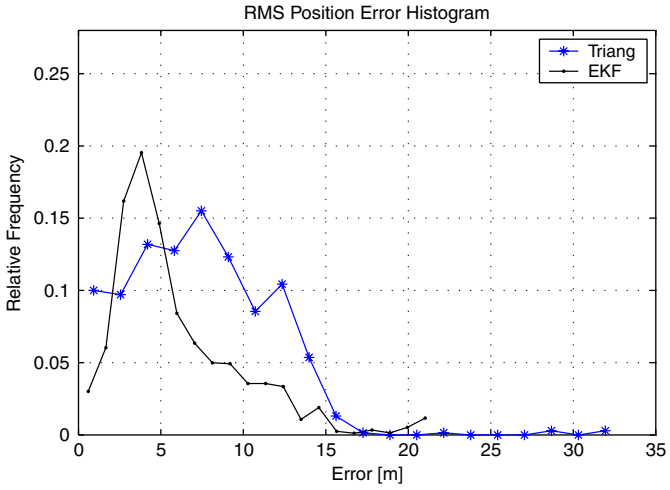

Fig. 18. RMS of position estimation errors of Triangulation and EKF compared to post-processed GPS.

8. Conclusions and future work

The paper proposed a solution to the problem of estimating the position of an underwater target in real time. The experimental setup adopted consists of a system of four buoys that compute the TOA of the acoustic signals emitted periodically by a pinger installed on-board the moving platform (so-called GIB system). The positioning system fuses the vehicle-to-buoy range measurements by resorting to an EKF-structure that addresses explicitly the problems caused by measurement delays. By dealing directly with each buoy measurement as it becomes available, a system was obtained that exhibits far better performance than that achievable with classical triangulation schemes, where all buoy measurements are collected before an estimate of the target's position can be computed. Simulation as well as experimental results show that the proposed filter is computationally effective and yields good results, even in the presence of acoustic outliers or a reduced number of valid buoy measurements. Future work will address the inclusion of a time-varying threshold in the time-domain validation strategy described as well as the study of other nonlinear filter structures for which convergence results can in principle be derived. Another interesting topic of research is how to extend the algorithm

Table 3
Main notation

$[x_{hi}(t)\ y_{hi}(t)\ z_{hi}(t)]^{\mathrm{T}}$	ith Hydrophone position at time t
$[x(t)\ y(t)\ z_p(t)]^{\mathrm{T}}$	Pinger position at time t
d_i	Distance between Pinger and ith hydrophone
$\mathbf{x}(t_k) = [x(t_k)\ y(t_k)\ V(t_k)\ \psi(t_k)\ r(t_k)]^{\mathrm{T}}$	Target state at time t_k
$\hat{\mathbf{x}}(t_k) = [\hat{x}(t_k)\ \hat{y}(t_k)\ \hat{V}(t_k)\ \hat{\psi}(t_k)\ \hat{r}(t_k)]^{\mathrm{T}}$	Filter state at time t_k
$\mathbf{A}(\mathbf{x}(t_k)), \mathbf{L}$	Target model state matrices
$\hat{\mathbf{A}}(\mathbf{x}(t_k)), \hat{\mathbf{L}}(\mathbf{x}(t_k)), \hat{\mathbf{C}}(\mathbf{x}(s)), \hat{\mathbf{D}}(\mathbf{x}(s))$	Filter Jacobian matrices
$\mathbf{w}(t_k)$	Process noise
$\mathbf{Q} = diag\{\sigma_v^2, \sigma_\psi^2, \sigma_r^2\}$	Process noise covariance matrix
$\mathbf{z}^m(s)$	Measurement vector (with first m measurements)
$\mathbf{v}^m(s)$	Measurement noise
$\mathbf{R}^m$	Measurement noise covariance matrix
$\mathbf{P}(t_k)$	Filter covariance matrix (a priori)
$\mathbf{P}^+(s)$	Filter covariance matrix (a posteriori)
$\mathbf{K}(s)$	Filter gain matrix
h	Filter time step size
T	Time between acoustic emissions
s	Time of an acoustic emission
t_k	Filter time tag

developed to AUV navigation, that is, how to fuse the filter estimates with other kinds of sensorial data by relaying AUV position estimates to the vehicle underwater using an acoustic communication channel.

Acknowledgments

We thank M. Rufino, L. Sebastião, J. Alves, G. Libório for their valuable help in setting up and operating the GPS and GIB equipments at sea and for their contribution to the development of some of the algorithms for data processing. We are also indebted to Prof. C. Silvestre for making available for the tests at sea the IRIS platform that was developed under the MEDIRES project.

This work supported in part by the Portuguese FCT (Foundation for Science and Technology) POSI Programme under framework QCA III, by project MAYA-Sub of the AdI, and by projects DREAM, MAROV, and RUMOS of the FCT. The work of the first author was supported by an EC research grant in the scope of the FREESUB Research Training Network and by a Ph.D. Scholarship of FCT.

References

ACSA, ORCA (1999). *Trajectographe GIB Manuel Utilisateur*.

Anderson, B. D. O., & Moore, J. B. (1979). *Optimal filtering*. Englewood Cliffs, NJ: Prentice-Hall.

Bar-Shalom, Y., & Fortmann, T. (1988). *Tracking and data association*. New York: Academic Press.

Henry, T. D. (1978). Acoustic transponder navigation. In *IEEE position location and navigation symposium* (pp. 237–244).

Jouffroy, J., & Opderbecke J. (2004). Underwater vehicle trajectory estimation using contracting PDE-based observers. In *Proceedings of the American control conference*, Boston, MA, USA.

Kinsey, J. C., & Whitcomb, L. L. (2003). Preliminary field experience with the DVLNAV integrated navigation system for manned and unmanned submersibles. In *Proceedings of the first IFAC workshop on guidance and control of underwater vehicles*, *GCUV*'03, Newport, South Wales, UK (pp. 83–88).

Larsen, M. B. (2001). *Autonomous navigation of underwater vehicles*. Ph.D. dissertation, Department of Automation, Technical University of Denmark.

Larsen, T. D., Poulsen, N. K., Andersen, N. A., & Ravn, O. (1998). Incorporation of time delayed measurements in a discrete-time Kalman filter. In *Proceedings of the 37th conference on decision and control*, Tampa, FL, USA (pp. 3972–3977).

Leonard, J., Bennett, A., Smith, C., & Feder, H. (1998). Autonomous underwater vehicle navigation. MIT Marine Robotics Laboratory Technical Memorandum 98-1.

Mili, L., Cheniae, M., Vichare, N., & Rousseeuw, P. (1996). Robust state estimation based on projection statistics. *IEEE Transactions on Power Systems*, *11*(2), 1118–1127.

Milne, P. H. (1983). *Underwater acoustic positioning systems*. Houston, TX: Gulf Publishing.

Silva, L., Santos, J., Neves, M., Silvestre, C., Oliveira, P., & Pascoal, A. (2003). Tools for the diagnosis and automated inspection of semi-submerged structures. In *13th international harbour congress*, Antwerpen, Belgium, March–April 2003.

Thomas, H. G. (1998). Gib buoys: An interface between space and depths of the oceans. In *Proceedings of IEEE autonomous underwater vehicles*, Cambridge, MA, USA (pp. 181–184).

Vaganay, J., Bellingham, J., & Leonard, J. (1996). Comparison of fix computation and filtering for autonomous acoustic navigation. In *Proceedings of the sixth IARP workshop on underwater robotics*, Toulon, La Seyne, France, 1996.

Vaganay, J., Leonard, J., & Bellingham, J. (1996). Outlier rejection for autonomous acoustic navigation. In *Proceedings of IEEE international conference on robotics and automation*, Minneapolis, MN, USA (pp. 2174–2181).

Whitcomb, L. L., Yoerger, D. R., & Singh, H. (1999). Combined Doppler/LBL based navigation of underwater vehicles. In *Proceedings of the 11th international symposium on unmanned untethered submersible technology*, Durham, NH, USA, August, 1999.

Youngberg, J. W. (1992). *Method for extending GPS to underwater applications*. US Patent 5,119,341, June 2, 1992.